ACS Catalysis

Research Article

pubs.acs.org/acscatalysis

Stabilization of Cobalt Catalysts by Embedment for Efficient Production of Valeric Biofuel

Peng Sun,[†,‡,§] Guang Gao,[†,§] Zelun Zhao,[†] Chungu Xia,[†] and Fuwei Li*[,†,‡]

[†]State Key Laboratory for Oxo Synthesis and Selective Oxidation, Lanzhou Institute of Chemical Physics, Chinese Academy of Sciences, Lanzhou 730000, P. R. China

[‡]Suzhou Institute of Nano-Tech and Nano-Bionics, Chinese Academy of Sciences, Suzhou 215123, P. R. China

Supporting Information

ABSTRACT: We herein report, for the first time, a bifunctional base-metal catalyst (Co@HZSM-5) that acts as an efficient alternative to noble-metal catalysts (e.g., Pt, Ru) for the conversion of levulinic acid into valeric biofuel under batch and fixed-bed reactor conditions. The cobalt nanoparticles were embedded in HZSM-5 crystals and catalyzed the sequential hydrogenations of the ketone and alkene functional groups; meanwhile, the acidic zeolite catalyzed the ring opening of the γ-valerolactone intermediate. Although base metals (e.g., Co) are abundant and inexpensive, their sintering and/or leaching under liquid-phase conditions always lead to the irreversible deactivation of the catalyst. In this system, the embedment structure stabilizes the nanoparticles, and Co@HZSM-5 could be used up to eight times. This work provides a practical clue toward the stabilization of base-metal catalysts and will inspire the development of large-scale biorefinery.

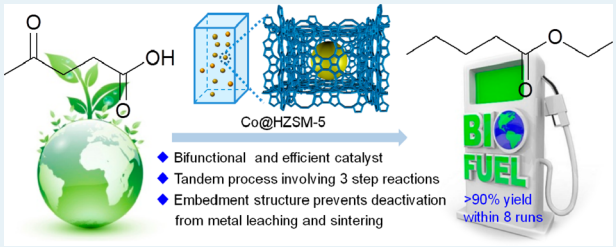

KEYWORDS: *biofuel, levulinic acid, valerate esters, cobalt, stability*

1. INTRODUCTION

Valerate esters have recently been recognized as a new class of cellulosic transportation fuels, called "valeric biofuels",[1] because they have acceptable energy densities and more appropriate polarities than many biofuel candidates such as ethanol and γ-valerolactone (GVL). Moreover, they are fully compatible for blending with gasoline or diesel and passed a 250 000 km road trial in 2010.[2,3] Since the first report on multistep production of valeric acid (VA) from levulinic acid (LA) over a Pt catalyst by Shell in 2010,[3] very few catalysts have been developed for the one-pot conversion of LA to VA/valerate esters. In 2013, Weckhuysen and co-workers[4] and Fu and co-workers[5] reported their pioneering works on the direct transformations of LA to VA in dioxane and ethyl valerate (EV) in ethanol, respectively, with different supported Ru catalysts. Unfortunately, catalyst deactivation due to the acid and/or metal leaching has not been properly solved. As elucidated in Scheme 1, GVL is an important intermediate in the direct conversion of LA to VA/valerate esters. Dumesic and co-workers developed a variety of efficient Pd/Nb_2O_5 catalysts for the transformation of GVL into VA,[6−9] and their systematic investigations showed that modification of the Nb_2O_5 catalyst by Nb−Si oxide,[7] Nb_2O_5/SBA-15-ALD,[8] and NbCe-C[9] could improve its catalytic stability.

Base metals (e.g., Co) are abundant and inexpensive, but sintering and/or leaching of base metals cause irreversible deactivation of the catalyst under liquid-phase conditions.[10] Therefore, the search for stable and efficient base-metal catalysts under liquid-phase reaction conditions remains an important challenge in the field of heterogeneous catalysis.[11]

Cobalt catalysts have found efficient applications in the well-known Fischer−Tropsch synthesis[12,13] and other hydrogenation reactions.[10,14] Herein we report for the first time that the

Scheme 1. Transformation of Levulinic Acid to Valeric Acid and Ethyl Valerate

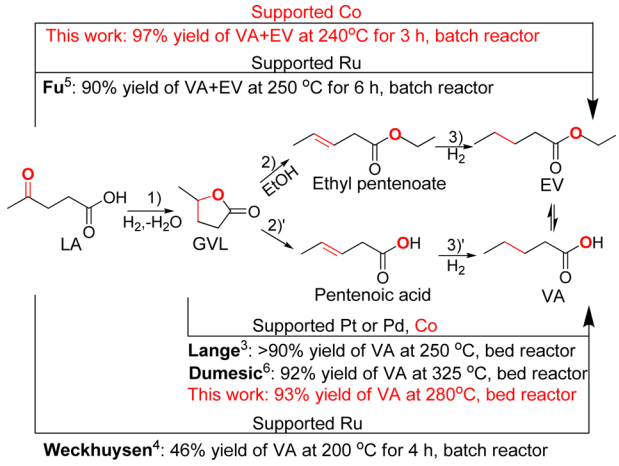

Received: September 17, 2014
Revised: October 9, 2014
Published: October 13, 2014

   dx.doi.org/10.1021/cs501409s | ACS Catal. 2014, 4, 4136−4142

base metal cobalt can replace noble metals in the one-pot production of EV/VA from LA with high catalytic activity and stability under batch and fixed-bed reactor conditions. By combining reaction studies and materials characterization, we elucidate how the embedment of cobalt nanoparticles in HZSM-5 zeolite crystals stabilizes the nanoparticles under liquid-phase conditions.

2. RESULTS AND DISCUSSION

2.1. Catalytic Behavior. The HZSM-5-supported Co catalyst (Co/HZSM-5) was prepared by incipient wetness impregnation. The catalyst consisting of cobalt nanoparticles embedded in HZSM-5 crystals (Co@HZSM-5) was obtained by an in situ synthetic strategy using Co_3O_4/SiO_2 as the precursor, in which the basicity of the system was controlled to dissolve the silica from Co_3O_4/SiO_2 at a proper rate and the contained Co_3O_4 particles served as substrates for the nucleation and growth of HZSM-5 crystals[15] (see the Experimental Section for details). The as-prepared samples with the same Co loading amount (10 wt %) were calcined at 500 °C for 5 h and subsequently reduced at 450 °C for 4 h. The catalytic performances of Co/HZSM-5 and Co@HZSM-5 were studied for the liquid-phase hydrogenation of LA to EV. This reaction was chosen because EV shows extremely high potential for applications in the biofuel field. Furthermore, LA is derived from the cellulose portion of biomass and is expected to increase with the development of biorefinery.[16]

Figure 1 shows the product distribution as a function of time on stream for LA conversion over Co/HZSM-5 at 240 °C.

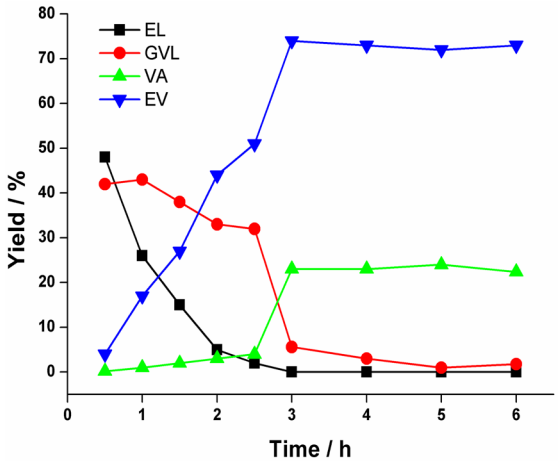

Figure 1. Time-course plot of LA conversion over Co/HZSM-5. Reaction conditions: LA, 1 g; catalyst, 0.1 g; ethanol, 6 mL; H_2, 3 MPa; 240 °C.

Complete conversion of LA could be achieved within 0.5 h, and the observed products were ethyl levulinate (EL) and GVL in 48% and 42% yield, respectively, implying that LA or EL could be quickly converted into GVL via hydrogenation of the ketone group and subsequent internal esterification (step 1 in Scheme 1). Moreover, the yield of VA and EV increased to 97% when the reaction time was prolonged to 3 h, suggesting that the bifunctional Co/HZSM-5 catalyst demonstrated good activity for the acid-catalyzed ring opening of GVL to give ethyl pentenoate (step 2 in Scheme 1) as well as the following hydrogenation to afford EV (step 3 in Scheme 1). Ethyl pentenoate was not detected in the product solution, possibly because its hydrogenation was faster than its production from GVL.[5]

When this reaction was performed at 210 °C, the major product was GVL, and VA and EV were obtained in a total yield of 15% (Table 1, entry 1), which was much lower than

Table 1. Catalytic Performance of Co/HZSM-5 for the Conversions of LA and GVL[a]

entry	catalyst	conv./%	selectivity/%		
			GVL	VA	EV
1	Co/HZSM-5[b]	100[c]	68	2	13
2	Co/HZSM-5	100[c]	1	23	74
3	Co/HZSM-5	93[d]	–	22	69
			4-EPE[f]	3-EPE[f]	2-EPE[f]
4	HZSM-5	45[d,e]	5	30	10

[a]Reaction conditions: LA or GVL, 1 g; catalyst, 0.1 g; ethanol, 6 mL; H_2, 3 MPa; 240 °C; 3 h. [b]210 °C. [c]LA conversion. [d]GVL conversion. [e]N_2, 3 MPa. [f]EPE is ethyl pentenoate, and its selectivity was determined by the area normalization method (55% of the GVL was left after the reaction).

that observed at 240 °C (97%; entry 2), indicating that the transformation of GVL to VA/EV is a temperature-sensitive reaction. To gain more details about this process, two controlled experiments were performed using GVL as the substrate at 240 °C in ethanol with Co/HZSM-5 or HZSM-5 as the catalyst (entries 3 and 4). GVL conversions of 93% and 45% were accordingly obtained, and the products were VA/EV and three ethyl pentenoate isomers, respectively. Such a big activity difference between the tandem reaction (steps 2 and 3) over Co/HZSM-5 and the single reaction (step 2) over HZSM-5 suggests that the bifunctionality of the Co/HZSM-5 catalyst is the crucial point for the efficient transformation of LA via the quick conversion to generate intermediates with different functionalities (GVL, pentenoic acid, and ethyl pentenoate) to afford the final VA/EV products. Moreover, comparisons with Ru, Pd, Cu, and Ni nanoparticles supported on HZSM-5 as reference catalysts showed that cobalt was equivalent to noble metals and far superior to other base metals for the conversion of LA to VA/EV (Table S1 in the Supporting Information).

Although it showed excellent catalytic performance, deactivation of Co/HZSM-5 during recycling was observed (Figure 2a). The yield of VA/EV dropped from 97% to 67% over the Co/HZSM-5 catalyst in its third run, while the GVL yield increased to 24%. However, the stability of Co@HZSM-5 obviously differed from that of Co/HZSM-5 under the same reaction conditions (Figure 2b). During eight runs, the Co@HZSM-5 catalyst showed outstanding stability in ethanol without obvious loss of LA conversion and product selectivity (>90% yield of VA/EV).

In view of the fact that LA is typically produced in water[17] while EV is the desired product, a water/ethanol mixture was used as the solvent. This protocol had the dual benefit of avoiding the fine separation of LA from water and affording the biofuel in one pot. Figure 3a displays the product distribution as a function of water content. When the water content in the initial solvent was less than 7.5 wt %, the yield of VA/EV remained above 90%. However, the yield decreased with increasing water content from 10 to 100 wt %, and GVL was the primary product in water, suggesting that LA could be completely converted into GVL but further GVL transformation was hindered in water. Thermodynamic calculations

dx.doi.org/10.1021/cs501409s | ACS Catal. 2014, 4, 4136−4142

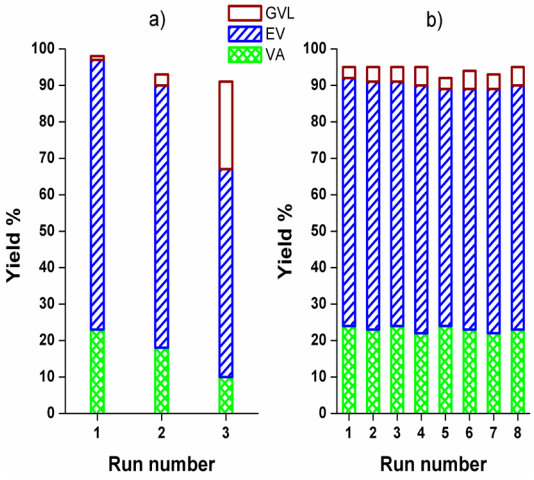

Figure 2. Reusability of (a) Co/HZSM-5 and (b) Co@HZSM-5 at full conversion of LA. Reaction conditions: LA, 1 g; catalyst, 0.1 g; ethanol, 6 mL; H_2, 3 MPa; 240 °C; 3 h.

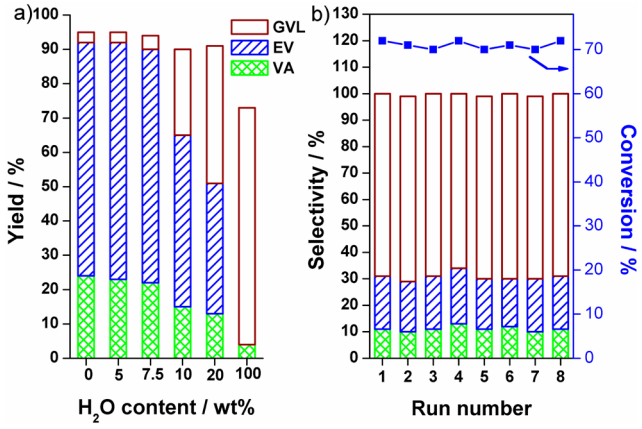

Figure 3. (a) Product distribution as a function of water content in water/ethanol solvent. Reaction conditions: LA, 1 g; Co@HZSM-5 catalyst, 0.1 g; solvent, 6 mL; H_2, 3 MPa; 240 °C; 3 h. (b) Reusability of Co@HZSM-5 in an environment containing 10 wt % water at about 70% conversion.

by Lange[18a] and Dumesic[18b] revealed a low free energy change (ΔG = +1.5 kJ mol^{-1}) for the conversion of GVL in MeOH but a higher ΔG (+25 kJ mol^{-1}) in water, indicating that the conversion of GVL in water is much more difficult than that in MeOH, consistent with our experimental results shown in Figure 3a. Gratifyingly, good catalytic activity and stability were achieved when the conversion of GVL into VA was conducted with water as the solvent in a fixed-bed reactor, as discussed below.

To further study the stability of the Co@HZSM-5 catalyst, recycling experiments in the presence of 10 wt % water (Figure 3b) and in neat LA (Figure S1 in the Supporting Information) were initially carried out in a batch reactor. The results demonstrated that the Co@HZSM-5 catalyst still possessed excellent recyclability in both the water-containing environment and neat LA. In addition, the stabilities of Co@HZSM-5 in ethanol (Figure S2) and water (Figure S3) were also tested in a continuous-flow reactor. The Co@HZSM-5-catalyzed LA conversion in ethanol and GVL transformation in water could stably run with >90% yield of VA/EV for 30 h and >80% yield of VA for 40 h, respectively, indicating that the as-prepared Co catalyst showed good catalytic activity and stability in both organic solvent and water. The deactivation of Co@HZSM-5 during long-term operation could be fully reversed by calcinations followed by reduction in H_2, which suggested that the deactivation was caused by coke deposits instead of sintering and leaching of Co. Transmission electron microscopy (TEM) (Figure 4d,e) and inductively coupled plasma atomic emission spectroscopy (ICP-AES) analysis further confirmed that sintering and leaching of Co did not occur.

To investigate the effects of residual impurities (e.g., formic acid and sulfuric acid) during the production of LA, extra formic acid and sulfuric acid were added. As shown in Table S2 and Figure S4, when the contents of formic acid and sulfuric acid in LA were less than 0.2% and 0.1%, respectively, the catalytic performance and stability of the Co@HZSM-5 was not influenced.

2.2. Structural Characterization. TEM was used to measure the particle size distributions of the cobalt nanoparticles before and after the reaction. For Co/HZSM-5, the Co nanoparticles were clearly located on the surface of HZSM-5 crystal, and the particle size was 25 ± 3 nm before the reaction and increased to 32 ± 4 nm after three cycles of reaction (Figure 4a,b). The Co/HZSM-5 lost up to 12.6 wt % of the original cobalt during 3 h from leaching, as detected by ICP-AES analysis (Table 2). These results showed that the HZSM-5-supported cobalt catalyst prepared by the impregnation method could not prevent the sintering and leaching of

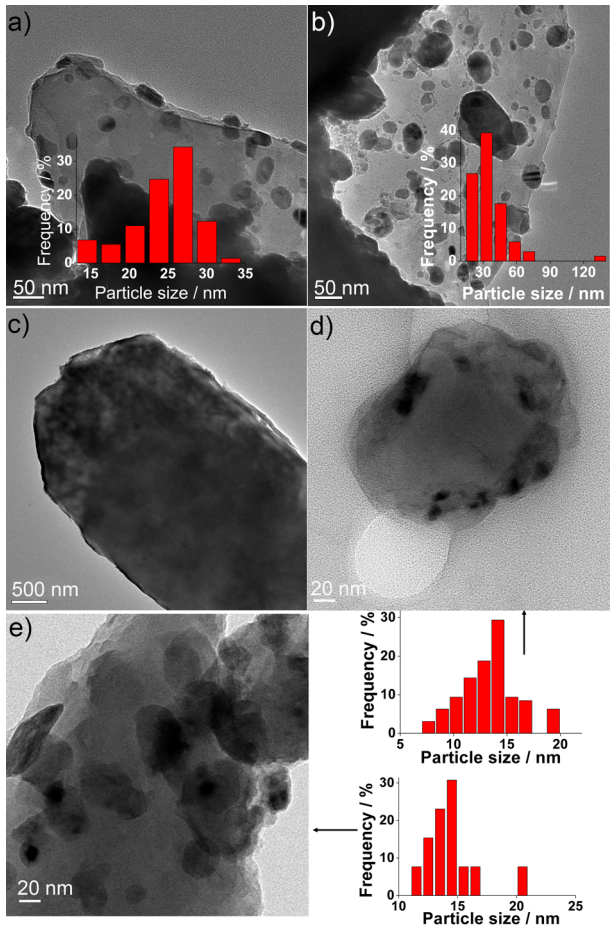

Figure 4. TEM images of (a) fresh Co/HZSM-5, (b) spent Co/HZSM-5, (c, d) fresh Co@HZSM-5, and (e) spent Co@HZSM-5.

dx.doi.org/10.1021/cs501409s | ACS Catal. 2014, 4, 4136−4142

Table 2. ICP-AES, TGA, N_2 Physisorption, H_2-TPR, H_2 Chemisorption, and NH_3-TPD Data for the Catalysts under Investigation

sample		cobalt leaching[a]/%	coke content[b]/wt %	S_{BET}[c]/m^2 g^{-1}	V_{pore}[c]/cm^3 g^{-1}	reducibility[d]/%	H_2 uptake[e]/μmol g^{-1}	acid amount[f]/μmol g^{-1}
Co/HZSM-5	fresh	–	–	295	0.090	91	31.1	50
	spent, 3 h	12.6	3.6	214	0.075	–	–	48[g]
Co@HZSM-5	fresh	–	–	346	0.105	85	28.5	33
	spent, 3 h	0.1	0.9	319	0.098		–	32[g]

[a]Measured by ICP-AES. [b]Analyzed by TGA. [c]Brunauer–Emmett–Teller surface area, as measured from N_2 adsorption–desorption isotherms. [d]Calculated from areas of H_2-TPR patterns. [e]Determined by H_2 chemisorption. [f]Determined by NH_3-TPD. [g]Before NH_3-TPD analysis, the spent catalyst was calcined in air to remove the reaction residue and coke deposits.

cobalt. The formation of coke (3.6 wt %) on Co/HZSM-5 was observed by thermogravimetric analysis (TGA) (Table 2). In addition, the decreases in surface area and pore volume revealed by N_2 physisorption data (Table 2) also proved that coke formation on the catalyst surface had occurred. Therefore, it could be concluded that sintering and leaching of Co nanoparticles as well as coke formation on the Co/HZSM-5 surface resulted in the activity decline during recycling.

For Co@HZSM-5, the Co particles seemed to lie under the shadow of the HZSM-5 crystal (Figure 4c), and the particle size was 15 ± 1 nm before and after batch or continuous-flow reaction (Figure 4d,e). Furthermore, ICP-AES analysis of the reaction solution showed only 0.1% Co loss after reuse, indicating that the embedment structure prevented sintering and leaching of cobalt.

X-ray diffraction (XRD) patterns of the spent Co/HZSM-5 and Co@HZSM-5 samples were comparable to their fresh patterns (Figure 5), suggesting the zeolites could maintain their

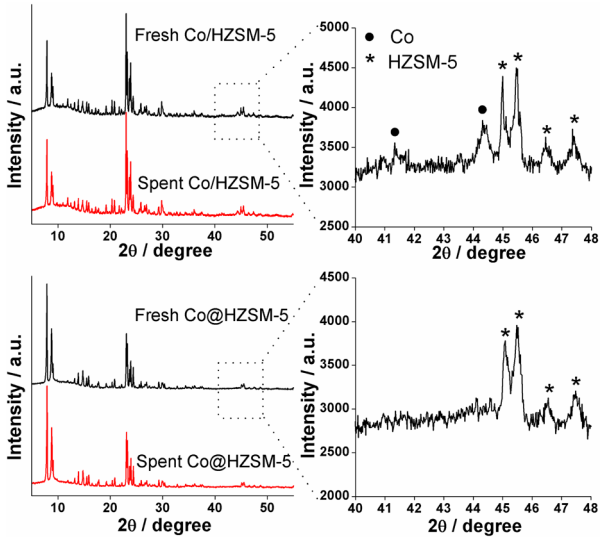

Figure 5. XRD patterns of fresh and spent Co/HZSM-5 and Co@HZSM-5.

structural integrity during the reaction. Closer inspection of the fresh XRD pattern of Co/HZSM-5 revealed two peaks at 41.4° and 44.5° assignable to the Co phase (PDF no. 05-0727),[19] while the Co@HZSM-5 sample displayed only the typical pattern of HZSM-5 and no Co characteristic peaks were observed, implying that the Co particles were small and homogeneously dispersed.[20]

Scanning electron microscopy (SEM) and elemental analysis were employed to probe the embedment structure. The SEM image of the Co@HZSM-5 sample (Figure 6a) showed the classical morphology of ZSM-5 zeolites, indicating that good

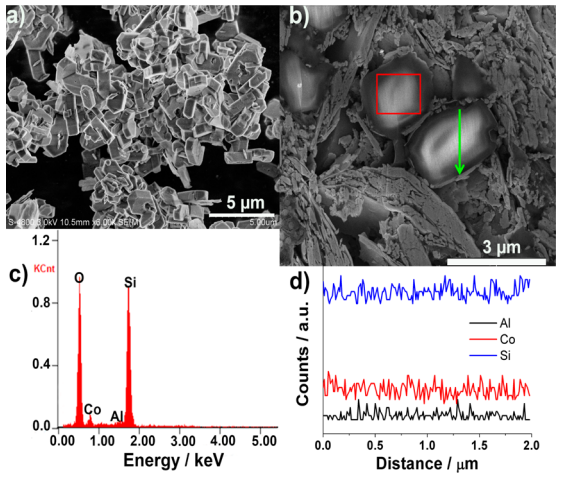

Figure 6. (a) SEM image of Co@HZSM-5. (b) Cross-sectional SEM image of Co@HZSM-5 crystals. (c) Elemental analysis of the red square region in (b). (d) EDS line scan along the green arrow through the cross section in (b).

uniformity and crystallinity of the sample were obtained using the in situ synthesis methodology. The embedment of Co nanoparticles in HZSM-5 crystal was verified by the cross-sectional SEM image (Figure 6b), which was obtained by Ar^+ etching of the sample using an Ilion Precision Cross-Section System.[21] Elemental analysis of the cross-section (red square region) indicated the coexistence of Si, Al, and Co within the crystal (Figure 6c). The energy-dispersive X-ray spectroscopy (EDS) line scan profile through the cross-section of a HZSM-5 crystal (Figure 6d) showed that the signal intensities of Si, Al, and Co along the green arrow remained almost constant, suggesting that Co nanoparticles were uniformly embedded in the HZSM-5 crystal.

One may speculate that the embedment structure of Co@HZSM-5 will give rise to a disadvantage in exposing the Co particles. In our case, calcinations of the as-prepared Co@HZSM-5 at 500 °C removed the organic template and produced porosity in the outer HZSM-5 framework, thereby providing access to the underlying cobalt nanoparticles. Hydrogen temperature-programmed reduction (H_2-TPR) and H_2 chemisorption were used to test the accessibility of Co particles for Co/HZSM-5 and Co@HZSM-5. Furthermore, H_2-TPR is a powerful tool to study the interaction between the supported phase and the carrier. As displayed in Figure 7, two closely spaced reduction peaks, assignable to the reduction of Co_3O_4 to CoO and the subsequent reduction of CoO to Co^0,[22]

dx.doi.org/10.1021/cs501409s | ACS Catal. 2014, 4, 4136–4142

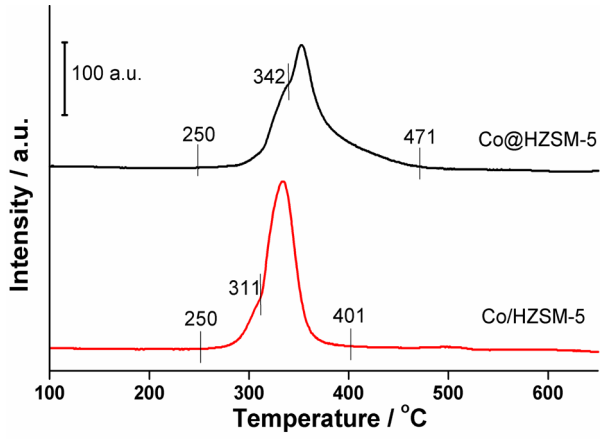

Figure 7. H_2-TPR profiles of Co/HZSM-5 and Co@HZSM-5.

were observed for both of the samples. The temperature maximum for Co@HZSM-5 (353 °C) is higher than that for Co/HZSM-5 (333 °C), indicating a stronger interaction between Co and the support.[23] The corresponding reducibilities calculated from areas (250−500 °C) of the H_2-TPR profiles were 91% and 85% for Co/HZSM-5 and Co@HZSM-5, respectively (Table 2). Moreover, the H_2 uptake for Co@HZSM-5 as determined by H_2 chemisorption was slightly less than that for Co/HZSM-5 (Table 2). In a word, the porous HZSM-5 capsule in Co@HZSM-5 afforded a stronger Co−support interaction but had little effect on the accessibility of the encapsulated Co nanoparticles in comparison with the postloaded Co/HZSM-5.

The ^{27}Al magic-angle spinning (MAS) NMR spectrum of Co@HZSM-5 revealed a single peak centered at about 54 ppm assigned to tetrahedrally coordinated aluminum (Figure 8),[24]

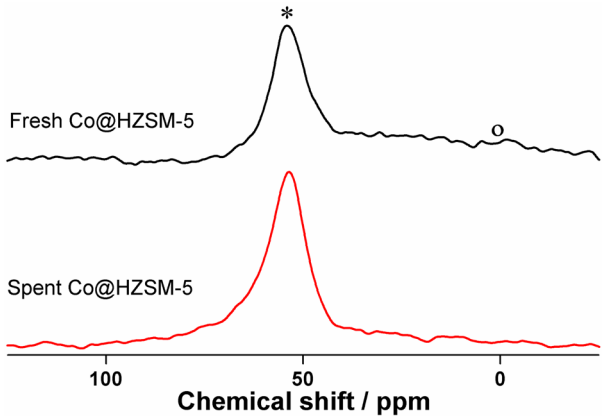

Figure 8. ^{27}Al MAS NMR spectra of the fresh and spent Co@HZSM-5 samples. * denotes tetrahedral aluminum, and O indicates octahedral aluminum.

indicating that the Al atoms were successfully incorporated into the zeolite framework and then endowed the bifunctional Co@HZSM-5 catalyst with acidity. After reaction in water/ethanol solvent, the tetrahedrally coordinated aluminum structure of the zeolites was maintained perfectly. The acid amounts of fresh and spent Co@HZSM-5 were lower than those of the Co/HZSM-5 catalyst (Table 2), accounting for the smaller amount of coke deposition[25] (0.9 wt % as determined by TGA).

3. CONCLUSIONS

We have successfully developed Co@HZSM-5, the first stable base-metal solid catalyst for the one-pot conversion of LA into valeric biofuel. It was found that the hydrogenation and acid functionality of Co@HZSM-5 sequentially catalyze the three-step reaction from LA into VA/EV and thus increase the process efficiency cooperatively. Robust catalytic tests under batch and fixed-bed reactor conditions together with detailed catalyst characterizations indicated that the homogeneous embedment of cobalt nanoparticles in HZSM-5 zeolite crystals can stabilize the cobalt nanoparticles against sintering and leaching under liquid-phase conditions, even in the presence of water. Thus, this in situ strategy for catalyst stabilization should be useful in supplementing precious-metal catalysts with abundant base metals for a range of traditional and biorenewable applications, where catalyst stability is still a challenge. This study also opens a practical clue for the cost-effective conversion of biobased feedstocks into biofuels.

4. EXPERIMENTAL SECTION

4.1. Preparation of the Catalysts. The HZSM-5-supported Co catalyst (Co/HZSM-5) was prepared by incipient wetness impregnation using an aqueous solution of $Co(NO_3)_2{\cdot}H_2O$ and commercial HZSM-5 zeolite (Si/Al = 38). The as-prepared sample was calcined at 500 °C for 5 h and reduced at 450 °C for 4 h. The Co loading amount was 10 wt %.

The catalyst consisting of cobalt nanoparticles encapsulated in HZSM-5 crystals (Co@HZSM-5) was obtained by an in situ synthetic strategy following a reported procedure with modifications.[15] Initially, the Co_3O_4/SiO_2 seed sample with a Co loading of 10 wt % was prepared by incipient wetness impregnation using an aqueous solution of $Co(NO_3)_2{\cdot}H_2O$ and commercial SiO_2 and then calcined at 400 °C. Subsequently, the Co@HZSM-5 catalyst was prepared by the following hydrothermal procedure: tetrapropylammonium hydroxide (TPAOH) was selected as the structure-directing agent, and the TPAOH:EtOH:$Al(NO_3)_3$:SiO_2:H_2O:NH_3 molar ratio was 15:500:1:38:1600:200. $Al(NO_3)_3{\cdot}9H_2O$ was first dissolved in H_2O and EtOH, after which the Co_3O_4/SiO_2 powder was added under stirring. Then TPAOH was added dropwise, and then the reaction mixture was further vigorously stirred at room temperature for 12 h. Finally, $NH_3{\cdot}H_2O$ was added to the solution, and the mixture was stirred for another 0.5 h. The autoclave was then sealed, and the mixture was hydrothermally crystallized at 180 °C for 100 h. After the autoclave was cooled, the product was separated by filtration and washed several times with deionized water and ethanol. The as-synthesized sample was dried at 120 °C for 12 h and then calcined at 500 °C for 5 h to remove the organic template. The obtained sample was reduced at 450 °C under H_2.

4.2. Characterization. TEM measurements were performed on an FEI Tecnai G2 F20 S-Twin electron microscope operated at an acceleration voltage of 200 kV. Metal leaching was measured by ICP-AES using an OPTIMA 3300 DV spectrometer (PerkinElmer, Norwalk, CT, USA). TGA was recorded using a Mettler-Toledo TGA/DSC 1 instrument; the samples were heated from room temperature to 800 °C at a heating rate of 10 °C min^{-1} with a gas feed (air) of 50 mL min^{-1}. XRD patterns were collected on a Bruker D8 Advance diffractometer using Cu Kα radiation (40 kV, 30 mA). N_2 physisorption was carried out on a Micromeritics TriStar II

dx.doi.org/10.1021/cs501409s | ACS Catal. 2014, 4, 4136−4142

3020 analyzer. All of the samples were outgassed at 250 °C for 4 h under vacuum to remove moisture and volatile impurities before the measurements. H_2-TPR was performed using a BEL-CAT-B-82 apparatus (BEL Japan Inc., Osaka, Japan). The temperature was increased from room temperature to 750 °C at a rate of 5 °C min^{-1} under a flow of 10% H_2/Ar (40 mL min^{-1}) after pretreatment at 300 °C. H_2 chemisorption was also performed on the BEL-CAT-B-82 instrument. Each sample was reduced in situ under a flow of H_2 at 450 °C, purged with He for 2 h, and cooled to 50 °C before the H_2 chemisorption; finally, 5% H_2/Ar pulses were injected into the sample tube until the hydrogen signal intensity was unchanged. NH_3 temperature-programmed desorption (NH_3-TPD) was performed on a XIANQUAN tp-5080 instrument (Tianjin, China) using the standard procedure. The morphology of the sample was investigated using a field-emission scanning electron microscope (Hitachi FESEM 4800). The cross section of the Co@HZSM-5 sample was prepared using an Ilion Precision Cross-Section System (model 693, Gatan Inc., Pleasanton, CA, USA). The sample was mixed with silver epoxy adhesive. One cross section was milled with an argon ion beam using an accelerating voltage of 4 kV for 2 h. The cross-sectional image was obtained by a field-emission scanning electron microscope (FEI, Quanta 400 FEG). ^{27}Al MAS NMR spectroscopy was conducted on a 300 MHz solid-state Bruker AV300 spectrometer (7.05 T), and the spectra were recorded at a frequency of 78.2 MHz.

4.3. Catalytic Reaction. In a typical reaction, the batch autoclave reactor was loaded with catalyst, substrate, and solvent, charged with H_2 to 3 MPa, and heated to the reaction temperature. After the reaction vessel was cooled to room temperature, the H_2 was released, and dioxane was added as an internal standard. The product samples were analyzed using a gas chromatograph (Agilent GC-7890A) equipped with an AT-SE-54 capillary column (60 m × 0.32 mm × 0.1 μm) and a flame ionization detector. Qualitative identification of products was achieved by GC−MS (Agilent 5975C/7890A). The spent catalyst was recovered from the reaction solution by centrifugation and washed three times with ethanol before it was recycled. The continuous-flow experiments were carried out using a fixed-bed reactor with an inner diameter of of 8 mm operated at 3 MPa H_2 pressure. The catalyst (2 g) was charged in the middle section of the reactor with quartz wool packed in both ends. Quartz sand (2 mL) was placed above the catalyst bed. Before the reaction, the catalyst was reduced at 450 °C under H_2 and cooled to the reaction temperature, and then the feedstock was pumped into the reactor.

■ ASSOCIATED CONTENT

Ⓢ Supporting Information

Tables S1 and S2 and Figures S1−S4. This material is available free of charge via the Internet at http://pubs.acs.org.

■ AUTHOR INFORMATION

Corresponding Author

*E-mail: fuweili@licp.cas.cn.

Author Contributions

§P.S. and G.G. contributed equally.

Notes

The authors declare no competing financial interest.

■ ACKNOWLEDGMENTS

This work was supported by the Chinese Academy of Sciences, the National Natural Science Foundation of China (21133011 and 21373246), the Natural Science Foundation of Jiangsu Province (BK20130354), and Jiangsu Planned Projects for Postdoctoral Research Funds (1202066C).

■ REFERENCES

(1) Palkovits, R. *Angew. Chem., Int. Ed.* **2010**, *49*, 4336−4338; *Angew. Chem.* **2010**, *122*, 4434−4436.

(2) Bozell, J. J. *Science* **2010**, *329*, 522−523.

(3) Lange, J.-P.; Price, R.; Ayoub, P. M.; Louis, J.; Petrus, L.; Clarke, L.; Gosselink, H. *Angew. Chem., Int. Ed.* **2010**, *49*, 4479−4483; *Angew. Chem.* **2010**, *122*, 4581−4585.

(4) Luo, W. H.; Deka, U.; Beale, A. M.; van Eck, E. R. H.; Bruijnincx, P. C. A.; Weckhuysen, B. M. *J. Catal.* **2013**, *301*, 175−186.

(5) Pan, T.; Deng, J.; Xu, Q.; Xu, Y.; Guo, Q. X.; Fu, Y. *Green Chem.* **2013**, *15*, 2967−2974.

(6) Serrano-Ruiz, J. C.; Wang, D.; Dumesic, J. A. *Green Chem.* **2010**, *12*, 574−577.

(7) Phama, H. N.; Pagan-Torres, Y. J.; Serrano-Ruiz, J. C.; Wang, D.; Dumesic, J. A.; Datye, A. K. *Appl. Catal., A* **2011**, *397*, 153−162.

(8) Pagán-Torres, Y. J.; Gallo, J. M. R.; Wang, D.; Pham, H. N.; Libera, J. A.; Marshall, C. L.; Elam, J. W.; Datye, A. K.; Dumesic, J. A. *ACS Catal.* **2011**, *1*, 1234−1245.

(9) Buitrago-Sierra, R.; Serrano-Ruiz, J. C.; Rodríguez-Reinoso, F.; Sepúlveda-Escribano, A.; Dumesic, J. A. *Green Chem.* **2012**, *14*, 3318−3324.

(10) Lee, J.; Jackson, D. H. K.; Li, T.; Winans, R. E.; Dumesic, J. A.; Kuech, T. F.; Huber, G. W. *Energy Environ. Sci.* **2014**, *7*, 1657−1660.

(11) O'Neill, B. J.; Jackson, D. H. K.; Crisci, A. J.; Farberow, C. A.; Shi, F.; Alba-Rubio, A. C.; Lu, J.; Dietrich, P. J.; Gu, X.; Marshall, C. L.; Stair, P. C.; Elam, J. W.; Miller, J. T.; Ribeiro, F. H.; Voyles, P. M.; Greeley, J.; Mavrikakis, M.; Scott, S. L.; Kuech, T. F.; Dumesic, J. A. *Angew. Chem., Int. Ed.* **2013**, *52*, 13808−13812; *Angew. Chem.* **2013**, *125*, 14053−14057.

(12) Bezemer, G. L.; Bitter, J. H.; Kuipers, H. P. C. E.; Oosterbeek, H.; Holewijn, J. E.; Xu, X.; Kapteijn, F.; van Dillen, A. J.; de Jong, K. P. *J. Am. Chem. Soc.* **2006**, *128*, 3956−3964.

(13) Wang, H.; Zhou, W.; Liu, J. X.; Si, R.; Sun, G.; Zhong, M. Q.; Su, H. Y.; Zhao, H. B.; Rodriguez, J. A.; Pennycook, S. J.; Idrobo, J. C.; Li, W. X.; Kou, Y.; Ma, D. *J. Am. Chem. Soc.* **2013**, *135*, 4149−4158.

(14) Vigier, K. D. O.; Pouilloux, Y.; Barrault, J. *Catal. Today* **2012**, *195*, 71−75.

(15) Liu, J. Y.; Chen, J. F.; Zhang, Y. *Catal. Sci. Technol.* **2013**, *3*, 2559−2564.

(16) Wright, W. R. H.; Palkovits, R. *ChemSusChem* **2012**, *5*, 1657−1667.

(17) Bozell, J. J.; Moens, L.; Elliott, D. C.; Wang, Y.; Neuenscwander, G. G.; Fitzpatrick, S. W.; Bilski, R. J.; Jarnefeld, J. L. *Resour. Conserv. Recycl.* **2000**, *28*, 227−239.

(18) (a) Lange, J.-P.; Vestering, J. Z.; Haan, R. J. *Chem. Commun.* **2007**, 3488−3490. (b) Bond, J. Q.; Alonso, D. M.; West, R. M.; Dumesic, J. A. *Langmuir* **2010**, *26*, 16291−16298.

(19) Zhou, H. C.; Song, J. L.; Fan, H. L.; Zhang, B. B.; Yang, Y. Y.; Hu, J. Y.; Zhu, Q. G.; Han, B. X. *Green Chem.* **2014**, *16*, 3870−3875.

(20) (a) Wang, Y.; Guo, L. F.; Ling, Y.; Liu, Y. M.; Li, X. H.; Wu, H. H.; Wu, P. *Appl. Catal., A* **2010**, *379*, 45−53. (b) Fouad, O. A.; Mohamed, R. M.; Hassan, M. S.; Ibrahim, I. A. *Catal. Today* **2006**, *116*, 82−87.

(21) (a) Lin, J.; He, W.; Vilayurganapathy, S.; Peppernick, S. J.; Wang, B.; Palepu, S.; Remec, M.; Hess, W. P.; Hmelo, A. B.; Pantelides, S. T.; Dickerson, J. H. *ACS Appl. Mater. Interfaces* **2013**, *5*, 11590−11596. (b) Liu, F.; Sun, K.; Li, W.; Yan, C.; Cui, H.; Jiang, L.; Hao, X.; Green, M. A. *Appl. Phys. Lett.* **2014**, *104*, No. 051105.

(22) Prieto, G.; Martínez, A.; Murciano, R.; Arribas, M. A. *Appl. Catal., A* **2009**, *367*, 146−156.

(23) Martínez, A.; López, C.; Márquez, F.; Díaz, I. *J. Catal.* **2003**, *220*, 486−499.
(24) Do, T. O.; Nossov, A.; Springuel-Huet, M. A.; Schneider, C.; Bretherton, J. L.; Fyfe, C. A.; Kaliaguine, S. *J. Am. Chem. Soc.* **2004**, *126*, 14324−14325.
(25) Sun, P.; Yu, D. H.; Fu, K. M.; Gu, M. Y.; Wang, Y.; Huang, H. *Catal. Commun.* **2009**, *10*, 1345−1349.